Applications of 3-D LCR Networks in the Design of 3-D Recursive Filters for Processing Image Sequences

Yuejin Zhang and Leonard T. Bruton, *Fellow, IEEE*

***Abstract*—Applications of three-dimensional (3-D) LCR prototype networks in the design of 3-D recursive filters are reviewed and several types of new and useful 3-D LCR prototype filters are proposed and classified. These 3-D LCR prototype filters can be used to design 3-D recursive filters for the processing of image sequences involving 3-D spatio-temporal-domain Linear-Trajectory (LT) and Planar-Wave (PW) component signals. Among the new proposed filters, a 3-D Planar-Rejection (PR) filter can be used to reject an undesired spatially-varying or spatially-static background LT component signal; a 3-D Planar-Pass/Planar-Rejection (PP-PR) filter can be tuned to enhance a desired 3-D LT component signal and, at the same time, reject an undesired 3-D LT component signal.**

A technique for implementing the 3-D filter transfer functions is proposed that employs 3-D differential or 3-D integral operators, leading to highly-parallel and modular 3-D recursive filter structures that are efficient in computation. A simple design procedure is described and examples of image sequence processing are given.

I. Introduction

THE digital processing of image sequences is of increasing importance, due to rapid advances in computer and integrated circuit technologies and the growing demand for time-varying visual information.

Digital image sequences may be considered as three-dimensional (3-D) spatio-temporal-domain signals [1]–[4]. A large number of algorithms have been proposed for such applications as the enhancement, identification, and tracking of moving (i.e. spatially-dynamic) objects contained within such 3-D signals, [1]–[7]. Applications of these algorithms are in such areas as seismic signal processing, medical diagnostics, computer vision and telecommunications.

Linear and nonlinear 3-D digital filter algorithms have been used to enhance 3-D spatio-temporal-domain signals, [1]–[10]. In this contribution, we consider the use of 3-D linear shift-invariant recursive digital filters for enhancing 3-D signal objects. Such filters have been used for this purpose and have been found to have low complexity, a high-level of concurrency and fast operating speed [1], [2], [8]–[10]. Recently, design methods for these filters have been proposed that are based on 3-D continuous-domain passive networks, such as 3-D LCR networks, [1], [2], [4], [8]–[12], and on symmetries in 3-D transfer functions [13]–[14]. A significant advantage of designing 3-D recursive filters from 3-D LCR prototype networks is that the resulting filters are guaranteed to be Practical-BIBO stable [15].

Manuscript received October 8, 1993; revised January 20, 1994. This paper was recommended by John W. Woods and was supported in part by Micronet, the Federal Centre of Excellence on Microelectronic Devices, Circuits and Systems, and the Natural Science and Engineering Research Council of Canada.

The authors are with the Department of Electrical and Computer Engineering, University of Calgary, Calgary, Alberta, Canada.

IEEE Log Number 9400888.

A. Review of 3-D Continuous-Spatio-Temporal-Domain Linear-Trajectory (LT) and Planar-Wave (PW) Signals

A number of important 3-D filtering problems, associated with the enhancement of digitized image sequences, involve 3-D component signals that can be characterized in the 3-D continuous-spatio-temporal-domain ($\mathbf{t} \equiv [\mathbf{t_1}, \mathbf{t_2}, \mathbf{t_3}]^{\mathbf{T}} \in \Re^3$) as Linear-Trajectory (LT) or Planar-Wave (PW) signals [1]. For example, 3-D motion estimation, applied to High Definition Television (HDTV), is effectively based on the assumption that the signal can be spatially divided into blocks and that the signal in each block approximates a 3-D LT signal.

A 3-D signal $x(\mathbf{t})$ is a LT signal if there exists a direction in $\mathbf{t}$, defined by the unit trajectory vector $\mathbf{d}_{\mathrm{LT}} \equiv [d_1, d_2, d_3]^T \in \Re^3$, along which $x(\mathbf{t})$ is constant; that is, the directional derivative $\partial x(\mathbf{t})/\partial \mathbf{d}_{\mathrm{LT}}$ is zero. Such signals have the property, when presented as a temporal succession of frames in t_3, that they move with constant spatial velocity [1] [16] given by

$$v_{12} \equiv \frac{\sqrt{d_1^2 + d_2^2}}{d_3} \tag{1}$$

Many practical 3-D images contain component 3-D images that approximate LT signals. For example, the human vision system prefers to process dynamic signals that appear to exhibit temporally-smooth motion, implying that such moving signals may be approximated by piece-wise LT signals. An example of a cylindrically-shaped 3-D LT signal $x(\mathbf{t})$ is given in Fig. 1(a) and, when viewed as a sequence of frames, appears as a smoothly moving ellipse, as shown in Fig. 1(b).

A 3-D continuous-spatio-temporal-domain Planar-Wave (PW) signal is an important special case of a 3-D LT signal, and has the property that the signal is constant in each of the infinite number of planes

$$\beta^T \mathbf{t} = c, \; c \in \Re^1 \tag{2}$$

defined by different values of c, where $\beta \equiv [\beta_1, \beta_2, \beta_3]^T \in \Re^3$. For example, the 3-D complex exponential signal

$$x(\mathbf{t}) = \exp(j\beta^T \mathbf{t}) \tag{3}$$

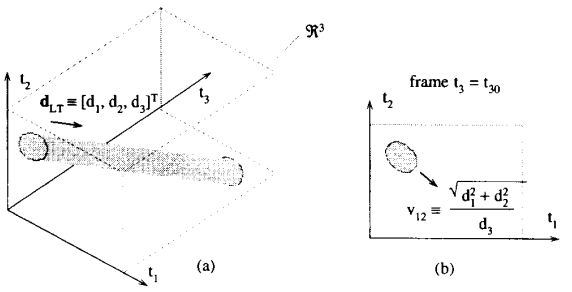

Fig. 1. 3–D LT signal object: (a): a cylindrically-shaped LT signal x(**t**) in **t** ϵ $\Re^3$ and (b) the elliptical shape in $(t_1$–$t_2)$ ϵ $\Re^2$.

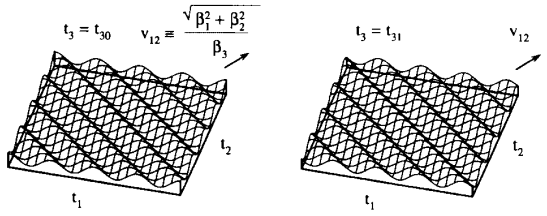

Fig. 2. The real part of a 3-D complex PW exponential signal exp(j j^T**t**) viewed in two planes of constant t_3.

is a complex 3-D PW signal having a constant value for every value of c in the planes given by (2).

The real part of the 3-D PW signal (3) is shown in Fig. 2, which is obviously a 3-D sinusoidal signal having spatial velocity

$$v_{12} \equiv \frac{\sqrt{\beta_1^2 + \beta_2^2}}{\beta_3}. \tag{4}$$

B. Review of the Spectral Representation of 3-D LT and PW Signals

The Fourier Transform of 3-D LT Signals: Consider a coordinate system $\mathbf{u} \equiv [u_1, u_2, u_3]^T \in \Re^3$ representing a LT signal $x_u(\mathbf{u})$, chosen so that *the 3-D unit trajectory vector* $\mathbf{d}_{u\mathrm{LT}}$ *points in the direction of the* u_3 *axis;* thus $\mathbf{d}_{u\mathrm{LT}} = [0, 0, 1]^T$. Then, a LT signal having a different trajectory can be obtained by rotating the signal $x_u(\mathbf{u})$. Hence, the rotated signal $x(\mathbf{t})$ can be represented in the new coordinate system **t** by the transformation

$$\mathbf{t} = \mathbf{R}_3\mathbf{u} \tag{5}$$

so that

$$x(\mathbf{t}) = x_u(\mathbf{R}_3^T\mathbf{t}), \tag{6}$$

where $\mathbf{R}_3$ is a 3×3 orthogonal matrix. In the coordinate system **u**, $x_u(\mathbf{u}) = f(u_1, u_2)$ is only a function of u_1, u_2 and has the 3-D Fourier transform

$$\begin{aligned} X_u(j\Omega) &\equiv \int_{-\infty}^{+\infty} x_u(\mathbf{u}) e^{-j\Omega^T\mathbf{u}} d\mathbf{u} \\ &= \delta(j\Omega_3) \int_{-\infty}^{+\infty}\int_{-\infty}^{+\infty} f(u_1, u_2) e^{-j(\Omega_1 u_1 + \Omega_2 u_2)} du_1 du_2 \end{aligned} \tag{7}$$

which has the region of support given by the plane

$$\Omega_3 = 0, \tag{8}$$

where $\Omega \equiv [\Omega_1, \Omega_2, \Omega_3]^T \in \Re^3$ is the 3-D frequency domain corresponding to **u**.

It is well known [1] that the rotation $\mathbf{t} = \mathbf{R}_3\mathbf{u}$ implies the same rotation of the 3-D Fourier transform so that, with

$$X(j\omega) \equiv \int_{-\infty}^{+\infty} x(\mathbf{t}) e^{-j\omega^T\mathbf{t}} d\mathbf{t}, \tag{9}$$

$$X(j\omega) = X_u(j\mathbf{R}_3^T\omega), \tag{10}$$

and where $\omega \equiv [\omega_1, \omega_2, \omega_3]^T \in \Re^3$. It follows from (8) and (10) that the region of support of the 3-D Fourier transform $X(j\omega)$ of a general 3-D LT signal $x(\mathbf{t})$ is given by the rotation of the plane (8) according to the transformation $\mathbf{R}_3$ [1]. Hence, *the 3-D Fourier transform* $X(j\omega)$ *of a LT signal is contained in a plane passing through the origin* [1]. It can be shown that a normal of the plane is given by $\mathbf{d}_{\mathrm{LT}} = \mathbf{R}_3\mathbf{d}_{u\mathrm{LT}}$.

The Fourier Transform of 3-D PW Signals: We rotate the coordinate system $\mathbf{u} = \mathbf{R}_3^T\mathbf{t}$ in such a way that each of the planes given by (2) is in parallel with the plane

$$u_3 = 0. \tag{11}$$

The Fourier transform $X_u(j\Omega)$ of the rotated PW signal $x_u(\mathbf{u})$ is given by

$$\begin{aligned} X_u(j\Omega) &\equiv \int_{-\infty}^{+\infty} x_u(\mathbf{u}) e^{-j\Omega^T\mathbf{u}} d\mathbf{u} \\ &= \delta(j\Omega_1)\delta(j\Omega_2) \int_{-\infty}^{+\infty} f(u_3) e^{-j\Omega_3 u_3} du_3, \end{aligned} \tag{12}$$

having a region of support that is the Ω_3 axis, where $f(u_3)$ is only a function of u_3. It follows from (10) and (12) that *the 3-D Fourier transform* $X(j\omega)$ *of a 3-D PW signal has a region of support on a straight line passing through the origin* [1].

II. Classes of 3-D Transfer Functions for the Processing of Image Sequences

Let the 3-D Laplace transform transfer function of a continuous-domain linear system be $T(\mathbf{s})$ and let the corresponding transform pairs of the 3-D input $x(\mathbf{t})$ and 3-D output $y(\mathbf{t})$ be $X(\mathbf{s})$ and $Y(\mathbf{s})$, respectively, where $\mathbf{s} \equiv [s_1, s_2, s_3]^T \in \mathbf{C}^3$. The corresponding 3-D steady-state frequency response is $T(j\omega)$ and the corresponding 3-D magnitude response $M(\omega)$. We are concerned here with the design of 3-D s-domain LCR networks that, after transformation to the discrete domain, lead to *useful* 3-D recursive filter algorithms for the enhancement of image sequences.

To facilitate the introduction of a class of useful 3-D LCR prototype networks, we employ the concept of 3-D inductance elements and 3-D capacitance elements. Assuming zero initial conditions, the series connection of transform inductance elements in Fig. 3(a) represents the j^{th} branch of a network and has the 3-D transform impedance

$$\mathbf{s}^T\mathbf{L}_j = s_1L_{j1} + s_2L_{j2} + s_3L_{j3} \tag{13}$$

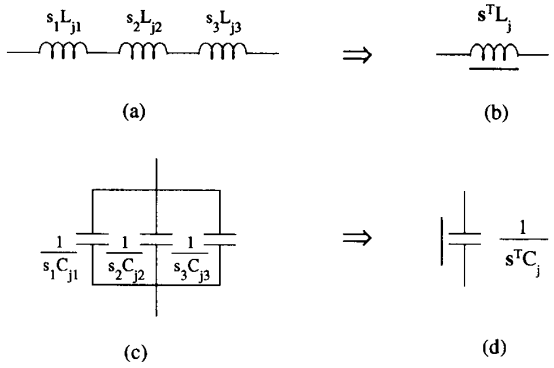

Fig. 3. 3-D series inductance and 3-D parallel capacitance and their elemental symbols.

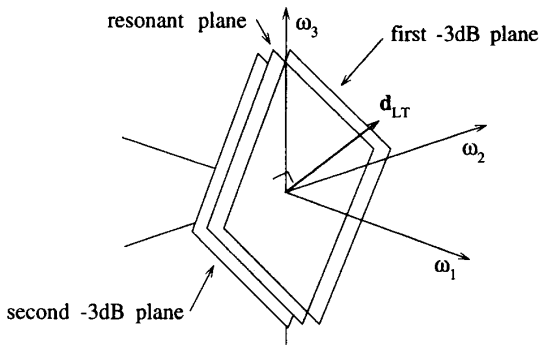

Fig. 4. The resonant plane, -3 dB planes, and $\mathbf{d}_{\mathrm{LT}}$ of PP1A prototype filter.

where $\mathbf{L}_j \equiv [L_{j1}, L_{j2}, L_{j3}]^T \in \Re^3$ and $L_{j1,2,3} \geq 0$. For simplicity, the elemental symbol shown in Fig. 3(b) is used to denote this 3-D series-inductance branch. Similarly, the 3-D parallel connection of transform admittances of a general j^{th} branch of a network has the transform admittance

$$\mathbf{s}^T\mathbf{C}_j = s_1C_{j1} + s_2C_{j2} + s_3C_{j3} \tag{14}$$

where $\mathbf{C}_j \equiv [C_{j1}, C_{j2}, C_{j3}]^T \in \Re^3$, $C_{j1,2,3} \geq 0$, and where the corresponding network is shown in Fig. 3(c). We use the elemental symbol in Fig. 3(d) for this type of 3-D parallel-capacitive branch.

Transform immittances of the types given in (13) and (14) are resonant (i.e. equal to zero) in $\omega \in \Re^3$ on the frequency plane

$$\omega^T\alpha_j = \omega_1\alpha_{j1} + \omega_2\alpha_{j2} + \omega_3\alpha_{j3} = 0 \tag{15}$$

where $\alpha_j = \mathbf{L}_j$ or $\alpha_j = \mathbf{C}_j$. *This property allows the following 3-D LCR prototype networks to be developed that selectively enhance and/or reject different LT component signals.*

A. 3-D LCR Networks Having Planar- and Beam-Shaped Passbands

Single-Passband Planar-Pass Networks: First, consider the known two 3-D LCR ladder networks in the first row of Table I, both of which have a first-order magnitude transfer function $M(\omega)$ that is characterized by a planar-shaped passband [1]. Clearly, the impedance of the series inductance element $\mathbf{L}_1$ in the filter type PP1A in Table I is zero in the frequency plane satisfying (15) and $M(\omega)$ is unity in this plane. Network PP1B is simply the network dual of PP1A. These types of networks have been used as continuous-domain prototype filters to realize highly selective discrete-domain 3-D recursive filters for the enhancement of passband LT signals in the presence of noise and in the presence of stopband LT signals [1], [8], [10]. Adaptive versions of such filters have been used to track objects that have nonlinear trajectories in the 3-D spatio-temporal domain [4].

It has been shown [1] that the trajectory of the passband LT signal in the spatio-temporal domain is given by the unit vector

$$\mathbf{d}_{\mathrm{LT}} = \mathbf{L}_1/\|\mathbf{L}_1\|_2. \tag{16}$$

so that the resonant plane (15) can be written in terms of $\mathbf{d}_{\mathrm{LT}}$ as

$$\omega^T\mathbf{d}_{\mathrm{LT}} = 0. \tag{17}$$

We call $\mathbf{d}_{\mathrm{LT}}$ in (16) the resonant trajectory of $\mathbf{L}_1$. The frequency-domain selectivity of network PP1A is increased by increasing $\|\mathbf{L}_1\|_2/R_L$ and is completely characterized by the 3-D Q factor [1]

$$Q(\omega) = \|\omega\|_2\|\mathbf{L}_1\|_2/R_L. \tag{18}$$

The continuous-domain surface contours of $M(\omega)$ are a set of planes, each of which is parallel to the resonant plane. The -3 dB planes have perpendicular distance $\|\omega\|_2/Q(\omega) = R_L/\|\mathbf{L}_1\|_2$ from the resonant plane. Typical surface contours of $M(\omega)$ are shown in Fig. 4.

Multiple-Passband Planar-Pass Networks: The networks PP1A and PP1B are now extended to include new networks possessing multiple planar-shaped passbands, *for the purpose of enhancing a number of LT component signals,* each having a different trajectory. This may be done by replacing $\mathbf{L}_1$ (in PP1A) by a parallel connection of such 3-D inductances, each having its resonant trajectory aligned to the trajectory of one of the LT component signals. (In the case of network PP1B, the 3-D capacitance $\mathbf{C}_1$ is replaced by a series connection of such capacitances, each aligned to the trajectory of a specific LT component signal). A second-order Double-passband Planar-Pass filter is shown as type DPP2A in Table I, where the equations $\omega^T\mathbf{L}_1 = 0$ and $\omega^T\mathbf{L}_2 = 0$ each define a passband plane and each of the passband planes allows a corresponding LT component signal to be selectively enhanced. (One of the reviewers has pointed out that the $\omega^T(\mathbf{L}_1 + \mathbf{L}_2) = 0$ is a rejection plane. Interestingly, this rejection plane is outside the region of the two planar-shaped passbands and therefore does not noticeably affect passband signals).

Beam-Pass Networks: It has been shown that 3-D beam-shaped passbands of $M(\omega)$, closely surrounding a straight line passing through the origin, may be realized *along the intersection of two passband resonant planes* [1]. 3-D ladder networks for achieving 3-D beam-shaped passbands have been proposed [2]. Two such known networks are shown as types BP2A and BP2B in Table I. For network BP2A, for example, the 3-D series inductance $\mathbf{L}_1$ in the series branch of the ladder provides the first passband resonant plane ($P_1 : \omega^T\mathbf{L}_1 = 0$)

TABLE I
3-D LCR PROTOTYPE FILTERS HAVING PLANAR PASS (PP) AND BEAM-PASS (BP) CHARACTERISTICS

Type	Topology	Transfer Function Characteristics	Applications
First-order Planar-Pass[1] (PP1)	(PP1A) 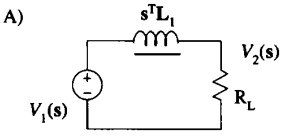 $T(s) = \frac{V_2(s)}{V_1(s)}$ ⇕ duality (PP1B) 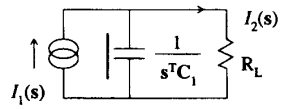 $T(s) = \frac{I_2(s)}{I_1(s)}$	$M(\omega) = 1$ in a plane where $\omega^T L_1 = 0$ for PP1A or $\omega^T C_1 = 0$ for PP1B	Enhancing a 3-D LT signal having the trajectory $\mathbf{d}_{LT} \propto \mathbf{L}_1$ for PP1A or $\mathbf{d}_{LT} \propto \mathbf{C}_1$ for PP1B
Second-order Beam-Pass[1] (BP2)	(BP2A) 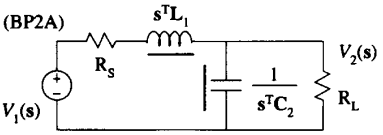 $T(s) = \frac{V_2(s)}{V_1(s)}$ ⇕ duality (BP2B) 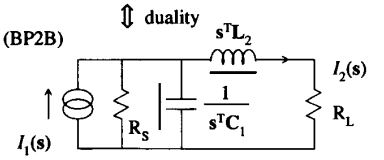 $T(s) = \frac{I_2(s)}{I_1(s)}$	$M(\omega) = 1$ in a passband line where $\omega^T L_1 = 0$, $\omega^T C_2 = 0$ for BP2A or $\omega^T C_1 = 0$, $\omega^T L_2 = 0$ for BP2B or	Enhancing a 3-D PW signal having the spectrum line $\frac{\omega_1}{\beta_1} = \frac{\omega_2}{\beta_2} = \frac{\omega_3}{\beta_3}$ that is aligned with the passband lines

Type	Topology	Transfer Function Characteristics	Applications
Second-order Beam-Pass (BP2)	(BP2C) 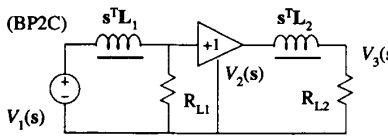 $T(s) = \frac{V_3(s)}{V_1(s)}$	$\omega^T L_1 = 0$, $\omega^T L_2 = 0$ for BP2C	and corresponds to a normal to the planar waves in t
Second-order Double-passband Planar-Pass (DPP2)	(DPP2A) 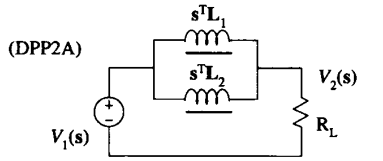 $T(s) = \frac{V_2(s)}{V_1(s)}$	$M(\omega) = 1$ in two planes where $\omega^T L_1 = 0$ or $\omega^T L_2 = 0$	Enhancing two 3-D LT signals having trajectories $\mathbf{d}_{LT1} \propto \mathbf{L}_1$ and $\mathbf{d}_{LT2} \propto \mathbf{L}_2$
Third-order Double-passband Beam-Pass (DBP3)	(DBP3B) 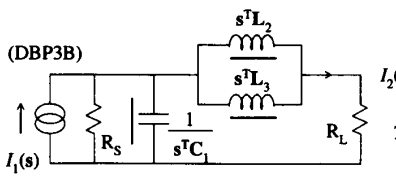 $T(s) = \frac{I_2(s)}{I_1(s)}$	$M(\omega) = 1$ in two passband lines where $\omega^T C_1 = 0$, $\omega^T L_2 = 0$ or $\omega^T C_1 = 0$, $\omega^T L_3 = 0$	Enhancing two 3-D PW signals having spectrum lines that are aligned with the two passband lines

and the 3-D parallel capacitance $\mathbf{C}_2$ in the shunt branch provides the second passband resonant plane ($P_2 : \omega^T \mathbf{C}_2 = 0$). The 3-D beam-shaped passband of $M(\omega)$ of the overall network surrounds the straight line that is the intersection of planes P_1 and P_2 [2]. Clearly, one may think of network BP2A (and its dual BP2B) in Table I as combining the resonant phenomena of the two types, PP1A and PP1B, into a single ladder structure. Networks of this type have been used as

prototypes to realize 3-D BP recursive filters for enhancing 3-D PW component signals [2].

Second-and Third-Order Networks Using Multiply-Aligned Resonant Planes: Second- and third-order versions of PP and BP LCR prototype networks may be designed *by employing the principle of multiply-aligned resonant planes.* A second-order cascade of PP1A networks results in the second-order type BP2C filter in Table I where, in this case, the beam-shaped passband surrounds the straight line at the intersection of the two resonant planes $\omega^T \mathbf{L}_1 = 0$ and $\omega^T \mathbf{L}_2 = 0$.

By combining the principle implied in the type PP1B filter with that in type DPP2A, one arrives at the type DBP3B filter in Table I; this is a third-order Double-passband Beam-Pass filter that is capable of selectively enhancing two PW component signals. The resonances are chosen so that the first PW component signal has its straight line spectrum at the intersection of the planes $\omega^T \mathbf{C}_1 = 0$ and $\omega^T \mathbf{L}_2 = 0$ and the second PW component signal has its straight line spectrum at the intersection of planes $\omega^T \mathbf{C}_1 = 0$ and $\omega^T \mathbf{L}_3 = 0$. The magnitude frequency response $M(\omega)$ has two beam-shaped passbands surrounding two straight lines passing through the origin. (We note that, for the type DBP3B filter, $\omega^T(\mathbf{L}_2 + \mathbf{L}_3) = 0$ is a rejection plane and that it is outside of the regions of the two beam-shaped passbands).

It is clear that one could generate higher-order PP and BP filters, employing additional series and shunt branches, following the above principles.

B. Zero Surface Planes and Planar-Rejection (PR) Filters

We say that a 3-D filter transfer function possesses the Planar-Rejection (PR) characteristic if its magnitude response $M(\omega)$ is zero in a 3-D frequency plane. Obviously, a 3-D PR filter ideally rejects a LT component signal if its spectrum lies in the zero surface plane. An important application of such filters is to reject a spatially-varying or spatially-static background LT component signal, which is difficult to remove using previously proposed 3-D filtering techniques, due to its very large energy at low frequencies.

Four new prototype 3-D PR LCR ladder filters are proposed and described in Table II. Type PR1A is of order one and selectively rejects a LT component signal having its spectrum in the plane $\omega^T \mathbf{C}_1 = 0$. Type PR1B is simply the dual network. Types PR2A and PR2B are of order two and are double Planar-Rejection filters; that is, they can reject two LT component signals having different trajectories because their $M(\omega)$ have two 3-D zero surface planes.

C. Combined Planar-Pass and Planar-Rejection Filters

Although one can readily envisage practical applications for the above PR filters involving the rejection of LT component signals, or simultaneously reject more than one LT component signals on more than one trajectory, the disadvantage of the PR filters is that they offer no control over the passband regions of the frequency space ω, which are where good planar-pass or beam-pass responses are often required.

Similarly, for PP and BP filters, planar-pass or beam-pass passband responses are obtained but the stopband attenuation is often insufficient.

In such cases, *the designer requires planar-shaped or beam-shaped passbands as well as planar-rejection surfaces.* This allows the selective enhancement of LT component signals and the simultaneous rejection of other LT component signals. The following combined PP-PR filters meet this more stringent task. Two LCR prototype ladder filter networks are proposed in Table III, both of which reject LT signals having a particular trajectory. Type PP-PR2A is a Planar-Pass/Planar-Rejection filter that is obtained by cascading two previously proposed filters. Clearly, it will selectively transmit a LT component signal having a spectrum in the resonant plane determined by the resonance of $\mathbf{L}_1$ and simultaneously reject a LT component signal having a spectrum in the zero surface determined by the resonance of $\mathbf{L}_2$. Type BP-PR3 is a third-order Beam-Pass/Planar-Rejection filter that selectively transmits a PW component signal while rejecting a LT component signal.

It should be noted that the rejection plane of the type PP-PR2A filter generally intersects the passband plane on a straight line so that the passband plane contains a non-ideal zero value along this line. In practice, this is usually not a problem because most LT passband signals will have spectra that are not significantly attenuated by removing their components on a single line.

Continuous-domain transfer function $T(\mathbf{s})$ of the 3-D LCR prototype filters can be transformed into the discrete domain by means of the 3-D bilinear transformation, leading to the corresponding discrete-domain transfer function

$$H(\mathbf{z}) = T(\mathbf{s})\Big|_{s_i = \frac{2}{T_i}\frac{1-z_i^{-1}}{1+z_i^{-1}}, i=1,2,3}. \tag{19}$$

The well known warping effect of the bilinear transformation distorts the shape of the passband in regions away from the origin where the assumptions

$$|\omega_i T_i| \ll \pi, \ i = 1, 2, 3 \tag{20}$$

do not hold. We do not address the 3-D frequency warping effect in this contribution and plan to consider this matter in a separate publication. For our purposes here, we assume that the signals of interest have 3-D spectra that are limited to the 3-D region given by (20), implying sufficient oversampling in all three dimensions.

III. Continuous-Domain SFG Implementations of 3-D Prototype Transfer Functions Using 3-D Differential and 3-D Integral Operators

We first note that the voltage transfer function $T(\mathbf{s}) = V_N(\mathbf{s})/V_1(\mathbf{s})$ of an N–branch ladder network of the type shown in Fig. 5 may be recursively written in terms of series branch impedances and shunt branch admittances [17]. The voltage transfer function of a four branch ladder network is given by [17]

$$T(\mathbf{s}) = \frac{V_4(\mathbf{s})}{V_1(\mathbf{s})} = \frac{1}{1 + Z_1[Y_2(1 + Z_3Y_4) + Y_4] + Z_3Y_4} \tag{21}$$

This four-branch prototype is sufficient for many 3-D filtering applications.

TABLE II
3-D LCR PROTOTYPE FILTERS HAVING PLANAR-REJECTION (PR) CHARACTERISTICS

Type	Topology		Transfer Function Characteristics	Applications
First-order Planar-Rejection (PR1)	(PR1A) 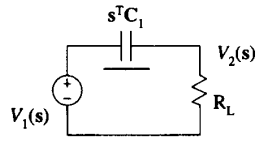 ⇕ duality (PR1B) 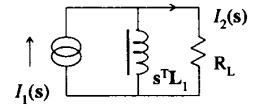	$T(s) = \frac{V_2(s)}{V_1(s)}$ $T(s) = \frac{I_2(s)}{I_1(s)}$	$M(\omega) = 0$ in a plane where $\omega^TC_1 = 0$ for PR1A or $\omega^TL_1 = 0$ for PR1B	Eliminating a 3-D LT signal having the trajectory $d_{LT} \propto C_1$ for PR1A or $d_{LT} \propto L_1$ for PR1B
Second-order Planar-Rejection (PR2)	(PR2A) 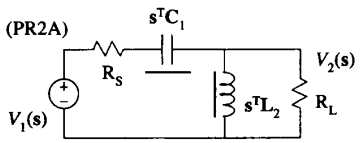 ⇕ duality (PR2B) 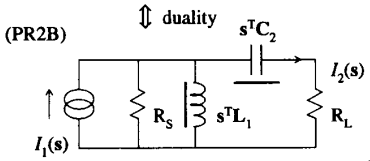	$T(s) = \frac{V_2(s)}{V_1(s)}$ $T(s) = \frac{I_2(s)}{I_1(s)}$	$M(\omega) = 0$ in two planes where $\omega^TC_1 = 0$ or $\omega^TL_2 = 0$ for PR2A and $\omega^TL_1 = 0$ or $\omega^TC_2 = 0$ for PR2B	Eliminating two 3-D LT signals having trajectories $d_{LT1} \propto C_1$, $d_{LT2} \propto L_2$ for PR2A and $d_{LT1} \propto L_1$, $d_{LT2} \propto C_2$ for PR2B

A technique for implementing the class of 3-D transfer functions T(s) obtained from the tabulated LCR prototype networks is proposed below and described for specific examples.

The Second-Order Beam-Pass BP2A Transfer Function: For the type BP2A prototype network, $Z_1 = R_S + \mathbf{s}^T\mathbf{L}_1$, $Y_2 = 1/R_L + \mathbf{s}^T\mathbf{C}_2$, and the voltage transfer function is given by

$$T(\mathbf{s}) = \frac{V_2(\mathbf{s})}{V_1(\mathbf{s})} = \frac{1}{1 + Z_1Y_2} = \frac{1}{1 + (R_s + \mathbf{s}^T\mathbf{L}_1)(1/R_L + \mathbf{s}^T\mathbf{C}_2)} \tag{22}$$

With $a_1 = \|\mathbf{L}_1\|_2/(R_S + R_L)$, $a_2 = R_L\|\mathbf{C}_2\|_2\|\mathbf{L}_1\|_2/(R_S + R_L)$, $a_3 = R_S/\|\mathbf{L}_1\|_2, b_0 = R_L/(R_S + R_L)$, and applying the inverse 3-D Laplace transform, equation (22) corresponds to the 3-D spatio-temporal t-domain equation

$$y(\mathbf{t}) + a_1D_1y(\mathbf{t}) + a_2D_2(a_3y(\mathbf{t}) + D_1y(\mathbf{t})) = b_0x(\mathbf{t}), \tag{23}$$

where $\mathbf{t} \equiv [t_1, t_2, t_3]^T \in \Re^3$ and where $D_j, j = 1, 2$, are 3-D t-domain *directional differential operators* (taken in the direction of propagation of the j^{th} LT surface $\mathbf{d}_{\text{LT}j} = \alpha_j/\|\alpha_j\|_2$) and are defined by

$$D_j[y(\mathbf{t})] \equiv \frac{\partial}{\partial \mathbf{d}_{\text{LT}j}}[y(\mathbf{t})] = \left(\frac{\partial}{\partial t_1}\cos\theta_{j1} + \frac{\partial}{\partial t_2}\cos\theta_{j2} + \frac{\partial}{\partial t_3}\cos\theta_{j3}\right)[y(\mathbf{t})]. \tag{24}$$

The directional cosines in (24) are given by $\cos\theta_{ji} = \alpha_{ji}/\|\alpha_j\|_2$, $j = 1, 2, i = 1, 2, 3$. From (24) and assuming zero initial conditions, the following 3-D Laplace transform (L^3) pair can be written

$$D_j[y(\mathbf{t})] \overset{L^3}{\Leftrightarrow} (s_1\cos\theta_{ji} + s_2\cos\theta_{j2} + s_3\cos\theta_{j3})Y(\mathbf{s}) = \mathbf{s}^T\mathbf{d}_{\text{LT}j}Y(\mathbf{s}) \tag{25}$$

where $Y(\mathbf{s})$ is the 3-D Laplace transform of $y(\mathbf{t})$.

The inverse operator D_j^{-1}, corresponding to D_j is a 3-D *directional integral operator* in $\mathbf{t}$ and, therefore, the following transform pair may be written

$$D_j^{-1}[y(\mathbf{t})] \overset{L^3}{\Leftrightarrow} (\mathbf{s}^T\mathbf{d}_{\text{LT}j})^{-1}Y(\mathbf{s}) \tag{26}$$

Remarks: By expressing the $\mathbf{t}$-domain (23) in terms of the 3-D operators it will be shown that the corresponding SFG realization of the 3-D filter can be derived in a straightforward way. It will also be shown that each of the 3-D operators D_j or $D_j^{-1}(j = 1, 2, 3)$ can be implemented using simple modular structures involving only three 1-D differentiators. Further, the final realization is particulary efficient in its use of multipliers.

For each j, both types of 3-D operators D_j and D_j^{-1} may be used to derive a SFG implementation of (23) and *the particular choice of operators leads to different filter structures.* Hereafter, we shall choose D_j or D_j^{-1} in such a way that the final SFG implementations are efficient in their use of multipliers. For brevity, we shall omit all of the rationale leading to our choice of operators.

TABLE III
3-D LCR PROTOTYPE FILTERS HAVING PP-PR OR BP-PR CHARACTERISTICS

Type	Topology	Transfer Function Characteristics	Applications
Second-order Planar-Pass / Planar-Rejection (PP-PR2)	(PP-PR2A) 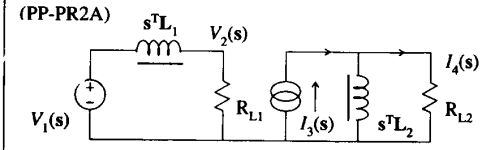 $T_1(s) = \frac{V_2(s)}{V_1(s)}$, $I_3(s) = V_2(s)/R_{L1}$, $T_2(s) = \frac{I_4(s)}{I_3(s)}$ $T(s) = T_1(s)T_2(s)$	$M(\omega) = 1$ in a plane $\omega^T L_1 = 0$ and $M(\omega) = 0$ in a plane $\omega^T L_2 = 0$	Enhancing a 3-D LT signal having the trajectory $\mathbf{d}_{LT1} \propto \mathbf{L}_1$ and eliminating a 3-D LT signal having the trajectory $\mathbf{d}_{LT2} \propto \mathbf{L}_2$ and
Third-order Beam-Pass / Planar-Rejection (BP-PR3)	(BP-PR3A) 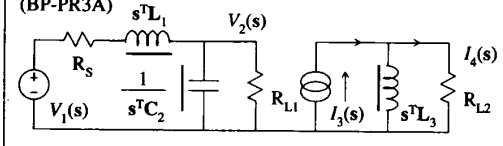 $T_1(s) = \frac{V_2(s)}{V_1(s)}$, $I_3(s) = V_2(s)/R_{L1}$, $T_2(s) = \frac{I_4(s)}{I_3(s)}$ $T(s) = T_1(s)T_2(s)$	$M(\omega) = 1$ in a passband line where $\omega^T L_1 = 0, \omega^T C_2 = 0$ and $M(\omega) = 0$ in a plane $\omega^T L_3 = 0$	Enhancing a 3-D PW signal and eliminating a 3-D LT signal having the trajectory $\mathbf{d}_{LT} \propto \mathbf{L}_3$

For the BP2A transfer function that is under consideration here, the differential operator D_j is used, rather than D_j^{-1}. With

$$x_{p1} \equiv D_1 y(\mathbf{t}), x_{p2} \equiv D_2(a_3 y(\mathbf{t}) + D_1 y(\mathbf{t})), \quad (27)$$

we obtain

$$\begin{aligned} y(\mathbf{t}) &= -a_1 x_{p1} - a_2 x_{p2} + b_0 x(\mathbf{t}) \\ D_1^{-1} x_{p1} &= y(\mathbf{t}) \\ D_2^{-1} x_{p2} &= a_3 y(\mathbf{t}) + x_{p1}. \end{aligned} \quad (28)$$

It is noticed that (28) is similar to a state-variable formulation except that x_{p1} and x_{p2} take the role of conventional state variables. This observation has motivated the proposed SFG implementation shown in Fig. 6.

If $\mathbf{d}_{LT1} = \mathbf{d}_{LT2}$, (23) corresponds to a second-order 3-D PP transfer function and can be written

$$y(\mathbf{t}) + a_4 D_1 y(\mathbf{t}) + a_2 D_1^2 y(\mathbf{t}) = b_0 x(\mathbf{t}), \quad (29)$$

where $a_4 = a_1 + a_2 a_3$. Clearly, the realization of (29) is effectively a 1-D *realization problem* except that the operators D_1 are *not* 1 – D differential operators, as in the conventional case. With

$$x_{p1} \equiv D_1 y(\mathbf{t}), \quad x_{p2} \equiv D_1^2 y(\mathbf{t}), \quad (30)$$

we have

$$y(\mathbf{t}) = -a_4 x_{p1} - a_2 x_{p2} + b_0 x(\mathbf{t})$$

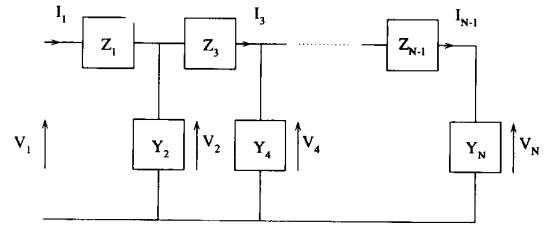

Fig. 5. An N-branch ladder network.

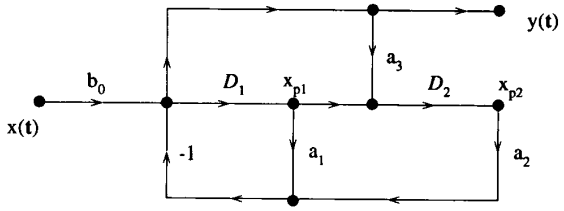

Fig. 6. A continuous-domain SFG realization of type BP2A filter.

$$\begin{aligned} D_1^{-1} x_{p1} &= y(\mathbf{t}) \\ D_2^{-1} x_{p2} &= x_{p1}, \end{aligned} \quad (31)$$

corresponding to the SFG shown in Fig. 7.

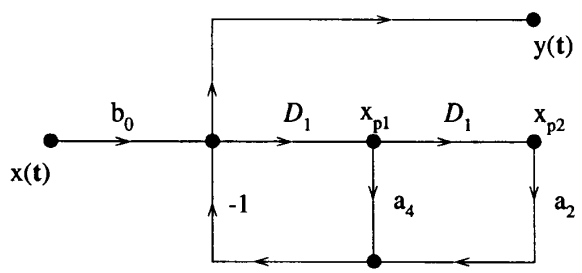

Fig. 7. A continuous-domain SFG realization of a second-order 3-D PP filter.

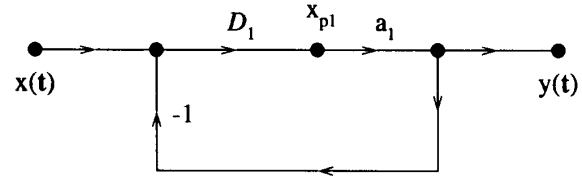

Fig. 8. A continuous-domain SFG realizations of type PR1A filter.

The First-Order Planar-Rejection PR1A Transfer Function For the type PR1A prototype network, $Z_1 = 1/\mathbf{s}^T\mathbf{C}_1, Y_2 = 1/R_L$, the voltage transfer function is

$$T(\mathbf{s}) = \frac{V_2(\mathbf{s})}{V_1(\mathbf{s})} = \frac{1}{1+Z_1Y_2} = \frac{R_L\mathbf{s}^T\mathbf{C}_1}{1+R_L\mathbf{s}^T\mathbf{C}_1}. \tag{32}$$

Let $a_1 = b_1 = R_L\|\mathbf{C}_1\|_2$ and apply the inverse 3-D Laplace transform to (32), resulting in the t-domain equation

$$y(\mathbf{t}) + a_1D_1y(\mathbf{t}) = b_1D_1x(\mathbf{t}). \tag{33}$$

Rearranging (33) gives

$$y(\mathbf{t}) = a_1D_1(x(\mathbf{t}) - y(\mathbf{t})). \tag{34}$$

With

$$x_{p1} \equiv D_1(x(\mathbf{t}) - y(\mathbf{t})), \tag{35}$$

we have

$$y(\mathbf{t}) = a_1x_{p1}, \tag{36}$$

yielding the SFG realization shown in Fig. 8.

The Second-Order Planar-Rejection PR2A Transfer Function For the type PR2A prototype network in Table II, $Z_1 = R_S + 1/\mathbf{s}^T\mathbf{C}_1$, $Y_2 = 1/R_L + 1/\mathbf{s}^T\mathbf{L}_2$, the voltage transfer function is

$$T(\mathbf{s}) = \frac{V_2(\mathbf{s})}{V_1(\mathbf{s})} = \frac{1}{1+Z_1Y_2} = \frac{1}{1+(R_s+1/\mathbf{s}^T\mathbf{C}_1)(1/R_L+1/\mathbf{s}^T\mathbf{L}_2)} \tag{37}$$

For implementing this transfer function, 3-D integral operators D_j^{-1} are chosen. With $a_1 = 1/[\|\mathbf{C}_1\|_2(R_S+R_L)]$, $a_2 = R_L/[\|\mathbf{C}_1\|_2\|\mathbf{L}_2\|_2(R_S+R_L)]$, $a_3 = R_S\|\mathbf{C}_1\|_2$, and $b_0 = R_L/(R_S+R_L)$, (37) corresponds to the 3-D t-domain equation

$$y(\mathbf{t}) + a_1D_1^{-1}y(\mathbf{t}) + a_2D_2^{-1}(a_3y(\mathbf{t}) + D_1^{-1}y(\mathbf{t})) = b_0x(\mathbf{t}). \tag{38}$$

Comparison of (23) and (38) shows that the two equations have the same structure except that the operators D_j in (23) are replaced by operators D_j^{-1} in (38). This implies an intrinsic relationship between BP2A and PR2A prototype networks. With

$$x_{p1} \equiv D_1^{-1}y(\mathbf{t}), \quad x_{p2}D_2^{-1}(a_3y(\mathbf{t}) + D_1^{-1}y(\mathbf{t})), \tag{39}$$

we have

$$\begin{aligned} y(\mathbf{t}) &= -a_1x_{p1} - a_2x_{p2} + b_0x(\mathbf{t}) \\ D_1x_{p1} &= y(\mathbf{t}) \\ D_2x_{p2} &= a_3y(\mathbf{t}) + x_{p1}, \end{aligned} \tag{40}$$

resulting in the SFG realization shown in Fig. 9.

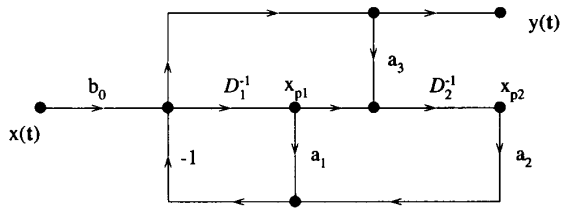

Fig. 9. A continuous-domain SFG realization of type PR2A filter.

Transfer Functions Having Multiply-Aligned Resonant Planes: As mentioned in Section II.A, this type of transfer function is derived from LCR networks that have 3-D inductances in parallel and/or 3-D capacitances in series and in a single branch. This particular configuration creates a special characteristic of their transfer functions. Consider the type DPP2A prototype network in Table I, in which $Z_1 = \mathbf{s}^T\mathbf{L}_1\mathbf{s}^T\mathbf{L}_2/(\mathbf{s}^T\mathbf{L}_1 + \mathbf{s}^T\mathbf{L}_2)$, $Y_2 = 1/R_L$, that has the voltage transfer function

$$T(\mathbf{s}) = \frac{V_2(\mathbf{s})}{V_1(\mathbf{s})} = \frac{1}{1+Z_1Y_2} = \frac{R_L(1/\mathbf{s}^T\mathbf{L}_1 + 1/\mathbf{s}^T\mathbf{L}_2)}{1+R_L(1/\mathbf{s}^T\mathbf{L}_1 + 1/\mathbf{s}^T\mathbf{L}_2)} \tag{41}$$

leading to the t-domain equation

$$y(\mathbf{t}) - a_1D_1^{-1}(x(\mathbf{t}) - y(\mathbf{t})) - a_2D_2^{-1}(x(\mathbf{t}) - y(\mathbf{t})) = 0 \tag{42}$$

where $a_1 = R_L/\|\mathbf{L}_1\|_2$ and $a_2 = R_L/\|\mathbf{L}_2\|_2$. With

$$x_{p1} \equiv D_1^{-1}(x(\mathbf{t}) - y(\mathbf{t})), \; x_{p2}\, D_2^{-1} \equiv 1(x(\mathbf{t}) - y(\mathbf{t})), \tag{43}$$

we obtain

$$\begin{aligned} y(\mathbf{t}) &= a_1x_{p1} + a_2x_{p2} \\ D_1x_{p1} &= x(\mathbf{t}) - y(\mathbf{t}) \\ D_2x_{p2} &= x(\mathbf{t}) - y(\mathbf{t}), \end{aligned} \tag{44}$$

giving the SFG realization shown in Fig. 10.

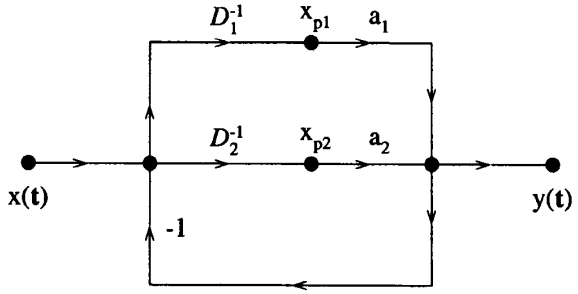

Fig. 10. A continuous-domain SFG realization of type DPP2A filter.

IV. Discrete-Domain SFG Implementations of 3-D LCR Prototype Transfer Functions

It is often necessary to implement these 3-D filters in the *discrete*-spatio-temporal domain $\mathbf{n} \equiv [n_1, n_2, n_3]^T$. It is known that 3-D Direct-Form (DF) structures [1], 3-D Wave Digital Filter (WDF) structures [2], [9], and 3-D Differentiator-type Ladder (DL) filter structures [8], [10] may be used to implement 3-D recursive filters. In particular, the 3-D DL structures have been shown to exhibit a high level of parallelism, allowing high-speed operation, as well as ease of tuning so that the resonant planes are easily aligned by appropriate modifications of the differentiator coefficients. However, the 3-D DL structures are not suitable for implementing some of the new 3-D filters proposed in Section II, because of the difficulty in eliminating the delay-free loops that are brought in by parallel 3-D inductors or serial 3-D capacitors within a single ladder branch.

In this section, we extend the 3-D continuous-domain implementation techniques of Section III to the discrete domain. The resulting 3-D discrete-domain recursive filter structures retain most of the advantages of 3-D DL structures and can be used to implement all the 3-D filters discussed in Section II. The proposed design procedures are straightforward, compared to that of 3-D DF, 3-D WDF, and 3-D DL structures. However, we point out that we make no claim concerning the retention of the almost-zero sensitivity property in the passband region, corresponding to maximum power transfer, that is often associated with 3-D WDFs and other pseudo-lossless structures that can be obtained from resistively terminated LCR prototypes via bilinear transformation.

A. Discrete-Domain 3-D Operators

Direct application of the 3-D bilinear transformation (BLT^3) cannot be used to convert the Laplace transformed versions of the continuous-domain SFGs into discrete-domain SFGs because discrete-domain versions of the 3-D operators

$$D_j[y(\mathbf{t})] \overset{L^3}{\Leftrightarrow} \mathbf{s}^T\mathbf{d}_{\mathrm{LT}j}Y(\mathbf{s}) \quad \mathrm{BLT}^3 \Leftrightarrow \left[\frac{2}{T_1}\frac{1-z_1^{-1}}{1+z_1^{-1}}, \frac{2}{T_2}\frac{1-z_2^{-1}}{1+z_2^{-1}}, \frac{2}{T_3}\frac{1-z_3^{-1}}{1+z_3^{-1}}\right]\mathbf{d}_{\mathrm{LT}j}Y(\mathbf{z}) \tag{45}$$

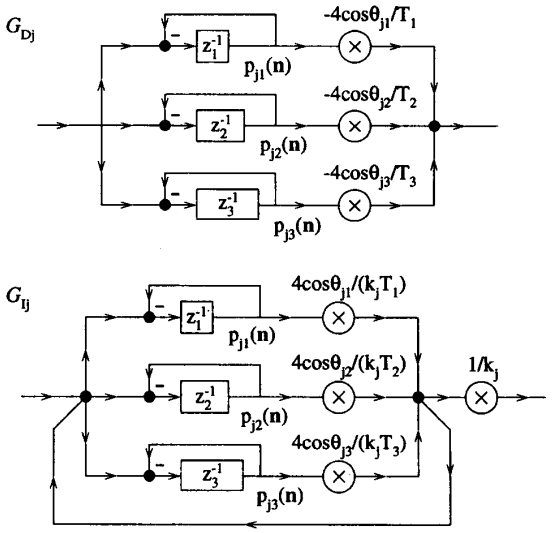

Fig. 11. Discrete-domain 3-D differential operator G_{Dj} and 3-D integral operator G_{Ij}.

$$D_j^{-1}[y(\mathbf{t})] \overset{L^3}{\Leftrightarrow} (\mathbf{s}^T\mathbf{d}_{\mathrm{LT}j})^{-1}Y(\mathbf{s}) \quad \mathrm{BLT}^3 \Leftrightarrow \left\{\left[\frac{2}{T_1}\frac{1-z_1^{-1}}{1+z_1^{-1}}, \frac{2}{T_2}\frac{1-z_2^{-1}}{1+z_2^{-1}}, \frac{2}{T_3}\frac{1-z_3^{-1}}{1+z_3^{-1}}\right]\mathbf{d}_{\mathrm{LT}j}\right\}^{-1}Y(\mathbf{z}) \tag{46}$$

have a delay-free forward path which, when incorporated into discrete-domain SFGs, leads to non-computable delay-free loops [18]. This difficulty is addressed below.

3-D Operators Without Delay-Free Forward Path: We define **n**-*domain* 3-D differential and 3-D integral operators G_{Dj} and G_{Ij} as follows

$$G_{Dj}[y(\mathbf{n})] \overset{Z^3}{\Leftrightarrow} \left[\frac{4}{T_1}\frac{-z_1^{-1}}{1+z_1^{-1}}, \frac{4}{T_2}\frac{-z_2^{-1}}{1+z_2^{-1}}, \frac{4}{T_3}\frac{-z_3^{-1}}{1+z_3^{-1}}\right]\mathbf{d}_{\mathrm{LT}j}Y_Z(\mathbf{z}) \quad \mathrm{BLT}^3 \Leftrightarrow (\mathbf{s}^T\mathbf{d}_{\mathrm{LT}j} - k_j)Y(\mathbf{s}) \tag{47}$$

$$G_{Ij}[y(\mathbf{n})] \overset{Z^3}{\Leftrightarrow} \left(\frac{1}{k_j}\frac{-G_{Dj}/k_j}{1+G_{Dj}/k_j}\right)Y_z(\mathbf{z}) \quad \mathrm{BLT}^3 \Leftrightarrow \left[(\mathbf{s}^T\mathbf{d}_{\mathrm{LT}j})^{-1} - \frac{1}{k_j}\right]Y(\mathbf{s}) \tag{48}$$

where (Z^3) implies the 3-D z transform, $Y_z(\mathbf{z}) = Z^3[y(\mathbf{n})]$ and the constant

$$k_j \equiv \left[\frac{2}{T_1}, \frac{2}{T_2}, \frac{2}{T_3}\right]\mathbf{d}_{\mathrm{LT}j} \in \Re^1 \tag{49}$$

It is easy to show that the above 3-D operators G_{Dj} and G_{Ij} correspond to the **n**-domain block diagram realizations shown in Fig. 11 and *have no delay-free forward path;* where z_i^{-1} represents a unit delay in the i^{th} dimension.

B. Procedures for Deriving 3-D Discrete-Domain SFGs from 3-D Prototype Transfer Functions

Based on the above results and techniques proposed in Section III, the following procedures can be employed to obtain discrete-domain SFG implementations of the prototype 3-D transfer functions $T(\mathbf{s})$.

Outline of the General Procedures: First, the designer chooses to use 3-D differential operators G_{Dj}, or 3-D integral operators G_{Ij} (or both) in the SFG implementations. For example, in order to achieve maximum savings in computation, operators G_{Dj} are suitable for implementing 3-D PP, 3-D BP, and first-order 3-D PR filters; operators G_{Ij} are suitable for implementing second-order 3-D PR, 3-D DPP, and 3-D DBP filters. Then, the prototype transfer function $T(\mathbf{s})$ is rearranged in such a way that the 3-D transform immittances appear in the form $\mathbf{s}^T\alpha_j$, corresponding to G_{Dj}, and/or $(\mathbf{s}^T\alpha_j)^{-1}$, corresponding to G_{Ij}.

Second, using the relationships between the continuous-domain 3-D transform immittances and the discrete-domain 3-D operators given by (47) and (48), the following substitutions are made

$$\begin{array}{|ll|}\hline \text{s-domain} & \text{n-domain} \\ \mathbf{s}^T\alpha_j = \|\alpha_j\|_2\mathbf{s}^T\mathbf{d}_{\mathrm{LT}j} & \|\alpha_j\|_2 G_{Dj} + \|\alpha_j\|_2 k_j \\ (\mathbf{s}^T\alpha_j)^{-1} = (\|\alpha_j\|_2\mathbf{s}^T\mathbf{d}_{\mathrm{LT}j})^{-1} & (\|\alpha_j\|_2)^{-1}G_{Ij} + (\|\alpha_j\|_2 k_j)^{-1} \\ T(\mathbf{s}) = V_N(\mathbf{s})/V_1(\mathbf{s}) & y(\mathbf{n})/x(\mathbf{n}) \\ \hline \end{array} \tag{50}$$

giving a corresponding $\mathbf{n}$-domain equation $F(x(\mathbf{n}), y(\mathbf{n}), G_{Dj}, G_{Ij})$.

Third, an $\mathbf{n}$-domain SFG implementation of $F(x(\mathbf{n}), y(\mathbf{n}), G_{Dj}, G_{Ij})$, consisting of 3-D operators G_{Dj} and/or G_{Ij}, multipliers, and adders, can be derived using the techniques proposed in Section III.

Finally, SFG identities may be used to simplify the resulting SFGs.

Stability and Initial Conditions: A significant advantage of designing M-D recursive filters from M-D LCR prototypes is that the resultant filters are guaranteed to be Practical-BIBO stable [15] under infinite precision arithmetic; that is, with zero initial conditions around the start-up boundary of the input and output signals, all spatially-bounded and amplitude-bounded signals $x(\mathbf{n})$ lead to output sequences $y(\mathbf{n})$ that are amplitude-bounded.

The zero initial condition in the 3-D filter,

$$y(\mathbf{n}) = 0, \quad n_1 < 0, n_2 < 0, n_3 < 0, \tag{51}$$

can be equivalently realized in all the 3-D operators G_{Dj} and G_{Ij} by ensuring that

$$\begin{cases} p_{j1}(\mathbf{n}) = 0, & n_1 = 0 \quad \text{(first columns)} \\ p_{j2}(\mathbf{n}) = 0, & n_2 = 0 \quad \text{(first rows)} \\ p_{j3}(\mathbf{n}) = 0, & n_3 = 0 \quad \text{(the first frame)} \end{cases} \tag{52}$$

where the variables $p_{ji}(\mathbf{n})$ are the output of delay elements in the i^{th} dimension, as illustrated in Fig. 11.

Implementations of Other Types of M-D Transfer Functions: The many different symmetries that often exist in M-D filter responses [13], [14] can lead to block-wise structures in the corresponding M-D transfer functions $T(\mathbf{s})$ or $H(\mathbf{z})$. For example, applying a spectral transformation $\mathbf{p} = g(s)$ to a 1-D prototype transfer function $\mathrm{T_p}$ yields many useful M-D prototype transfer functions $T(g(\mathbf{s}))$ [2], [19].

It is possible to generalize the above 3-D operators to M-D operators, that correspond to block-wise structures such as $g(\mathbf{s})$ above, for the implementation of other types of M-D transfer functions $T(\mathbf{s})$ or $H(\mathbf{z})$. For the case of transfer functions of the type $T(g(\mathbf{s}))$, operators G_D and/or G_I may be defined in the $\mathbf{n}$-domain to correspond to $(g(\mathbf{s}) + k_D)$ and/or $(g(\mathbf{s})^{-1} + k_I)$ in the $\mathbf{s}$-domain, where k_D and k_I are constants. This results in $\mathbf{n}$-domain equations $F(x(\mathbf{n}), y(\mathbf{n}), G_D, G_I)$ that can be implemented using the above proposed technique. Thus, the M-D implementation problem reverts to a 1-D implementation problem and therefore considerable savings in computation may be achieved.

C. Design Examples

To illustrate the proposed design procedures, some examples are given below for deriving $\mathbf{n}$-domain implementations of 3-D filters from their $\mathbf{s}$-domain prototype transfer functions $T(\mathbf{s})$.

The Second-Order Beam-Pass BP2A Transfer Function: Applying the transformations in (50) to the transfer function (22) yields the $\mathbf{n}$-domain equation

$$\begin{aligned} y(\mathbf{n})[1 + (R_S + \|\mathbf{L}_1\|_2 G_{D1} + \|\mathbf{L}_1\|_2 k_1) \\ \times (1/R_L + \|\mathbf{C}_2\|_2 G_{D2} + \|\mathbf{C}_2\|_2 k_2)] = x(\mathbf{n}). \end{aligned} \tag{53}$$

Let $r_1 = R_S + \|\mathbf{L}_1\|_2 k_1$, $r_2 = (1/R_L + \|\mathbf{C}_2\|_2 k_2)^{-1}$, and let $a_1 = \|\mathbf{L}_1\|_2/(r_1 + r_2)$, $a_2 = r_2\|\mathbf{C}_2\|_2\|\mathbf{L}_1\|_2/(r_1 + r_2)$, $a_3 = r_1/\|\mathbf{L}_1\|_2$, and $b_0 = r_2/(r_1 + r_2)$, giving

$$y(\mathbf{n}) + a_1 G_{D1} y(\mathbf{n}) + a_2 G_{D2}(a_3 y(\mathbf{n}) + G_{D1} y(\mathbf{n})) = b_0 x(\mathbf{n}). \tag{54}$$

Comparing (54) with (23), an $\mathbf{n}$-domain SFG implementation of the 3-D BP2A filter can be straightforwardly obtained. A simplified version of the implementation is shown in the block diagram in Fig. 12, where the multipliers are given by $m_0 = r_2/(r_1 + r_2)$, $m_1 = (r_1 + r_2)/r_1$, $m_{1i} = 4L_{1i}/[(r_1 + r_2)T_i]$, and $m_{2i} = 4C_2 i_1 r_2/[(r_1 + r_2)T_i]$, $i = 1, 2, 3$.

The First-Order Planar-Rejection PR1A Transfer Function: Applying the transformations in (50) to the transfer function (32) gives the $\mathbf{n}$-domain equation

$$\begin{aligned} y(\mathbf{n})(1 + R_L\|\mathbf{C}_1\|_2 G_{D1} + R_L\|\mathbf{C}_1\|_2 k_1) \\ = x(\mathbf{n})(R_L\|\mathbf{C}_1\|_2 G_{D1} + R_L\|\mathbf{C}_1\|_2 k_1). \end{aligned} \tag{55}$$

Let $a_1 = R_L\|\mathbf{C}_1\|_2/(1 + R_L\|\mathbf{C}_1\|_2 k_1)$ and $b_1 = R_L\|\mathbf{C}_1\|_2 k_1/(1 + R_L\|\mathbf{C}_1\|_2 k_1)$, giving

$$y(\mathbf{n}) - a_1 G_{D1}(x(\mathbf{n}) - y(\mathbf{n})) = b_1 x(\mathbf{n}) \tag{56}$$

corresponding to the simplified block diagram shown in Fig. 13, where the multipliers are given by $m_{1i} = 2R_L C_{1i}/[(1 + R_L\|\mathbf{C}_1\|_2 k_1)T_i]$, $i = 1, 2, 3$. The relationship $b_1 = m_{11} + m_{12} + m_{13}$ is used in the simplification.

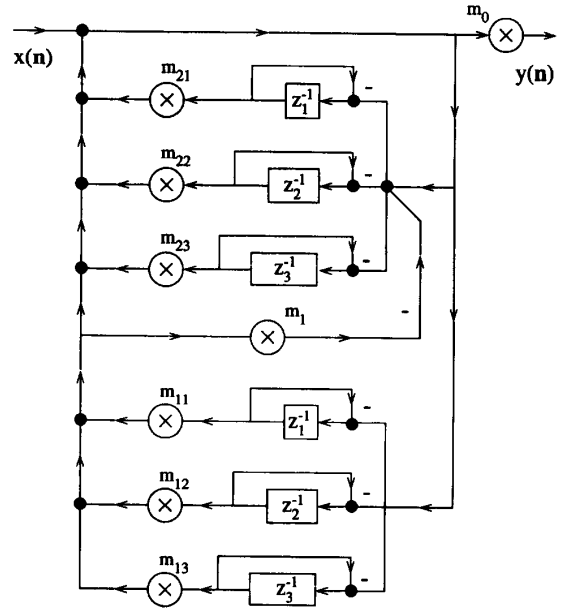

Fig. 12. A discrete-domain implementation of type BP2A filter.

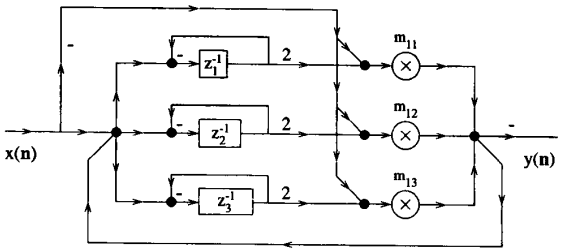

Fig. 13. A discrete-domain implementation of type PR1A filter.

The Second-Order Planar-Rejection PR2A Transfer Function: Applying the transformations in (50) to the transfer function (37) yields the **n**-domain equation

$$y(\mathbf{n})[1 + (R_S + \|\mathbf{C}_1\|_2^{-1}G_{I1} + \|\mathbf{C}_1\|_2^{-1}k_1^{-1}) \times (1/R_L + \|\mathbf{L}_2\|_2^{-1}G_{I2} + \|\mathbf{L}_2\|_2^{-1}k_2^{-1})] = x(\mathbf{n}). \quad (57)$$

Rearranging gives

$$y(\mathbf{n}) + a_1 G_{I1} y(\mathbf{n}) + a_2 G_{I2}(y(\mathbf{n}) + a_3 G_{I1} y(\mathbf{n})) = b_0 x(\mathbf{n}) \quad (58)$$

where $a_1 = 1/[\|\mathbf{C}_1\|_2(r_1 + r_2)]$, $a_2 = r_1 r_2/[\|\mathbf{L}_2\|_2(r_1 + r_2)]$, $a_3 = 1/(\|\mathbf{C}_1\|_2 r_1)$, and $b_0 = r_2/(r_1 + r_2)$, and where $r_1 = R_S + 1/(\|\mathbf{C}_1\|_2 k_1)$ and $r_2 = [1/R_L + 1/(\|\mathbf{L}_2\|_2 k_2)]^{-1}$. The corresponding block diagram is shown in Fig. 14, where $m_0 = r_2/(r_1 + r_2)$, $m_1 = 1/[\|\mathbf{C}_1\|_2 k_1(r_1 + r_2)]$, $m_2 = r_1 r_2/[\|\mathbf{L}_2\|_2 k_2(r_1 + r_2)]$, $m_3 = 1/(\|\mathbf{C}_1\|_2 k_1 r_1)$, $m_{1i} = 4C_{1i}/(\|\mathbf{C}_1\|_2 k_1 T_i)$, $m_{2i} = 4L_{2i}/(\|\mathbf{L}_2\|_2 k_2 T_i)$, and $i = 1, 2, 3$.

The Second-Order Double-Passband Planar-Pass DPP2A Transfer Function: Applying the transformations in (50) to the transfer function (41) gives the **n**-domain equation

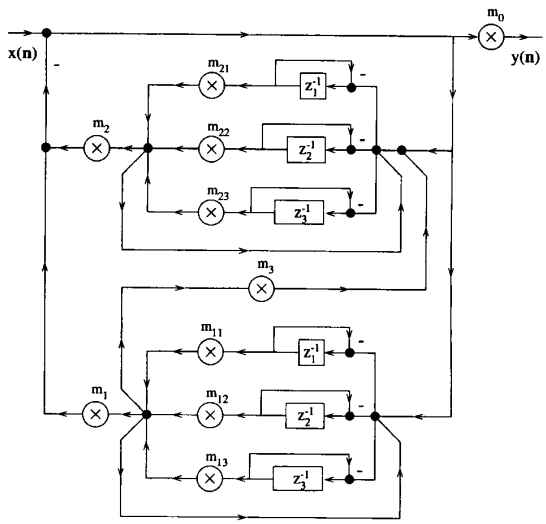

Fig. 14. A discrete-domain implementation of type PR2A filter.

$$y(\mathbf{n})(1 + R_L\|\mathbf{L}_1\|_2^{-1}G_{I1} + R_L\|\mathbf{L}_1\|_2^{-1}k_1^{-1} + R_L\|\mathbf{L}_2\|_2^{-1}G_{I2} + R_L\|\mathbf{L}_2\|_2^{-1}k_2^{-1}) = x(\mathbf{n})(R_L\|\mathbf{L}_1\|_2^{-1}G_{I1} + R_L\|\mathbf{L}_1\|_2^{-1}k_1^{-1} + R_L\|\mathbf{L}_2\|_2^{-1}G_{I2} + R_L\|\mathbf{L}_2\|_2^{-1}k_2^{-1}) \quad (59)$$

Let $K = 1 + R_L/(\|\mathbf{L}_1\|_2 k_1) + R_L/(\|\mathbf{L}_2\|_2 k_2)$, $a_1 = R_L/(\|\mathbf{L}_1\|_2 K)$, $a_2 = R_L/(\|\mathbf{L}_2\|_2 K)$ and $b_0 = (K-1)/K$, yielding

$$y(\mathbf{n}) - a_1 G_{I1}(x(\mathbf{n}) - y(\mathbf{n})) - a_2 G_{I2}(x(\mathbf{n}) - y(\mathbf{n})) = b_0 x(\mathbf{n}). \quad (60)$$

The block diagram realization of (60) is shown in Fig. 15, where $m_0 = b_0$, $m_1 = R_L/(\|\mathbf{L}_1\|_2 k_1 K)$, $m_2 = R_L/(\|\mathbf{L}_2\|_2 k_2 K)$, $m_{1i} = 4L_{1i}/(\|\mathbf{L}_1\|_2 k_1 T_i)$, $m_{2i} = 4L_{2i}/(\|\mathbf{L}_2\|_2 k_2 T_i)$, and $i = 1, 2, 3$.

V. Experimental Verifications

We have experimentally verified the operation of many of the proposed new 3-D recursive filter transfer functions and implementations. An image sequence $v_{i1}(\mathbf{n})$, having an 8-bit wordlength and consisting of 512 × 512 × 300 pixels, has been employed. The sequence $v_{i1}(\mathbf{n})$ consists of four groups of "shuttle" objects A, B, C, D, and a "painting" object E, as indicated by frames 150 and 300 in Fig. 16. The unit trajectory vectors of these objects are: $\mathbf{d}_A = [0.71, -0.071, 0.71]$, $\mathbf{d}_B = [0.33, -0.66, 0.66]$, $\mathbf{d}_C = [-0.70, -0.14, 0.70]$, $\mathbf{d}_D = [0.10, 0.24, 0.97]$ and $\mathbf{d}_E = [0.0, 0.0, 1.0]$, respectively. Note that the "painting" object E is spatially-static because its trajectory components are zero in both spatial directions n_1 and n_2. For ease of comparison, the objects on frame 300 of this sequence $v_{i1}(\mathbf{n})$, and of all following sequences, are also shown as shaded perspective 3-D views within each figure.

A second input image sequence $v_{i2}(\mathbf{n})$ has been created by adding random noise, uniformly distributed between 0 and

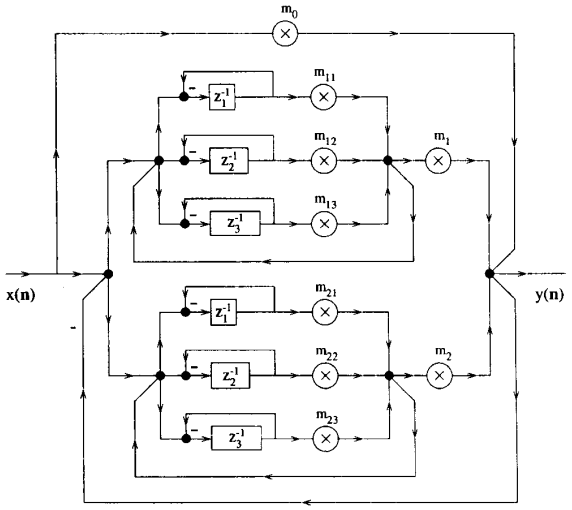

Fig. 15. A discrete-domain implementation of type DPP2A filter.

Fig. 16. Frames 150 and 300 of input sequence $v_{i1}(\mathbf{n})$.

Fig. 17. Frames 150 and 300 of noisy input sequence $v_{i2}(\mathbf{n})$.

255, to the sequence $v_{i1}(\mathbf{n})$. Frames 150 and 300 of the sequence $v_{i2}(\mathbf{n})$ are shown in Fig. 17.

Enhancement of Group A Objects: For enhancing group A, consisting of three "shuttle" objects, a 3-D recursive filter is designed based on the PP1A prototype network shown in

Fig. 18. Frames 150 and 300 of output sequence $v_{o1}(\mathbf{n})$ obtained using a PP1A prototype network.

Fig. 19. Frames 150 and 300 of output sequence $v_{o2}(\mathbf{n})$ obtained using a PP1A prototype network.

Fig. 12 in [10], with $L_{11} = 60$H, $L_{12} = 6$H, $L_{13} = 60$H, $R_L = 1\Omega$, and $T_1 = T_2 = T_3 = 1$ second (the same values of T_i are assumed hereafter), giving multiplier coefficients $m_{11} = 0.95, m_{12} = 0.095, m_{13} = 0.95$, and $m_0 = 0.004$ according to [10]. Frames 150 and 300 of the output sequences $v_{o1}(\mathbf{n})$ and $v_{o2}(\mathbf{n})$, corresponding to $v_{i1}(\mathbf{n})$ and $v_{i2}(\mathbf{n})$, are shown in Fig. 18 and Fig. 19, respectively.

Rejection of Group A Objects: For rejecting group A objects, a 3-D recursive filter is designed based on the PR1A prototype network by choosing $C_{11} = 60$F, $C_{12} = 6$F, $C_{13} = 60$F, and $R_L = 1\Omega$. The multiplier coefficients for the SFG in Fig. 13 are obtained according to Section IV. C and are given by $m_{11} = 0.4743, m_{12} = 0.04743, m_{13} = 0.4743$. Frames 150 and 300 of the output image sequence $v_{o1}(\mathbf{n})$, corresponding to $v_{i1}(\mathbf{n})$, are shown in Fig. 20. It is observed that group A objects, consisting of three "shuttles" and having the selected trajectory $\mathbf{d}_A$. are attenuated.

Enhancement of Group A Objects/Rejection of Object E: For enhancing group A objects while simultaneously rejecting the spatially-static "painting" object E, a 3-D recursive filter has been designed, based on the PP-PR2A prototype network. The parameters of the prototype are chosen as $R_{L1} = R_{L2} = 1\Omega$, $L_{11} = 60$H, $L_{12} = 6$H, $L_{13} = 60$H, $L_{21} = 0$H, $L_{22} = 0$ H, and $L_{23} = 60$ H. The multiplier coefficients can then be determined according to [10] and Section IV.C. Frames

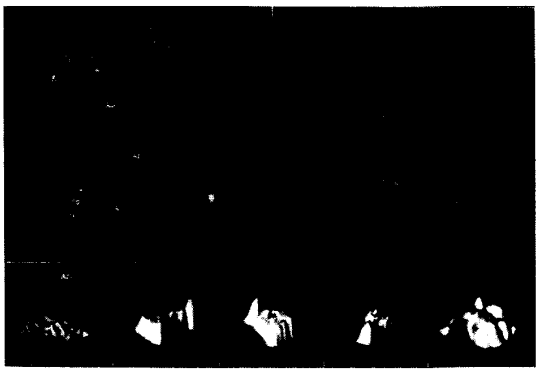

Fig. 20. Frames 150 and 300 of output sequence $v_{o1}(\mathbf{n})$ obtained using a PR1A prototype network.

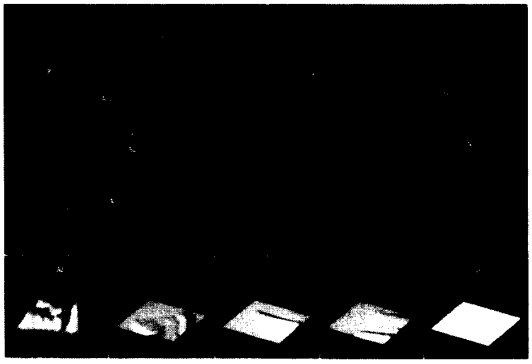

Fig. 21. Frames 150 and 300 of output sequence $v_{o1}(\mathbf{n})$ obtained using a PP-PR2A prototype network.

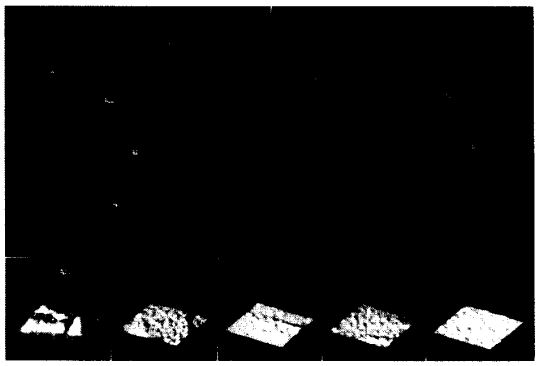

Fig. 22. Frames 150 and 300 of output sequence $v_{o2}(\mathbf{n})$ obtained using a PP-PR2A prototype network.

150 and 300 of the output image sequence $v_{o1}(\mathbf{n})$ and $v_{o2}(\mathbf{n})$, corresponding to $v_{i1}(\mathbf{n})$ and $v_{i2}(\mathbf{n})$, are shown in Fig. 21 and Fig. 22, respectively. As expected, the group A of "shuttle" objects is enhanced and the object E is attenuated.

By comparing the simulated results shown in Fig. 21 and Fig. 22 with those in Fig. 18 and Fig. 19, respectively, the advantage of PP-PR type filters over PP type filters is evident, showing the improved selective enhancement of the multiple LT component signals. In Fig. 18 and Fig. 19, the considerably large low-frequency energy of object E still exists after filtering; while in Fig. 21 and Fig. 22, this low-frequency energy is also significantly attenuated. In Fig. 22, the low-frequency energy of the additive random noise is also significantly attenuated, compared with that in Fig. 19.

VI. Conclusion

In the first part of this contribution, applications of 3-D LCR prototype networks for the design of 3-D recursive filters have been reviewed and additional new 3-D LCR prototype filters are proposed that employ multiple-passbands, for the concurrent enhancement of multiple linear-trajectory objects, and zero planar-surfaces for the rejection of linear trajectory objects. It is shown that these 3-D LCR prototype filters can be used to design useful and stable 3-D recursive filters for the processing of image sequences. Among the proposed 3-D filters, a 3-D Planar-Rejection (PR) filter is useful for the rejection of 3-D Linear-Trajectory (LT) and Planar-Wave (PW) component signals, such as a dynamic background signal and a 3-D Planar-Pass/Planar-Rejection (PP-PR) filter is especially useful in the enhancement of a 3-D LT component signal in the presence of other LT component signals.

A technique is proposed for implementing 3-D filters in both the continuous-domain and the discrete-domain that employs the concept of 3-D-differential and 3-D-integral operators. This technique results in algebraic decompositions that are similar to the conventional state-variable formulation and 3-D filter signal flowgraphs structures that are modular and efficient in their use of multipliers. A simple design procedure is described and experimental evidence is provided that demonstrate these new 3-D filters are useful.

References

[1] L. T. Bruton and N. R. Bartley, "Three-dimensional image processing using the concept of network resonance," *IEEE Trans. Circuits Syst.*, vol. CAS-32, pp. 664–672, Jul. 1985.

[2] Q. Liu and L. T. Bruton, "Design of 3D planar and beam recursive digital filter using spectral transformations," *IEEE Trans. Circuits Syst.*, vol. CAS-36, pp. 365–374, Mar. 1989.

[3] S. J. Ko and Y. H. Lee, "Nonlinear spatio-temporal noise suppression techniques with applications in image sequence processing," *Proc. IEEE ISCAS*, pp. 662–665, Jun. 1991.

[4] L. T. Bruton and N. R. Bartley, "Adaptive three-dimensional recursive filters applied to the enhancement and tracking of moving objects in digital images," *Proc. IEEE ISCAS*, pp. 1373–1376, Kyoto, Japan, Jun. 1985.

[5] S. D. Bolstein and T. S. Huang, "Detecting small, moving objects in image sequences using sequential hypothesis testing," *IEEE Trans. Signal Procsssing*, vol. SP-39, pp. 1611–1629, Jul. 1991.

[6] G. W. Donohoe, "Combining segmenta[illegible] and tracking for the classification of moving objects in video sc[illegible]," *IEEE Asilomar Conf. on Signals, Systems, and Computers, ACSSC 88*, vol. 2, pp. 533–537, Dec. 1988.

[7] D. D. Sworder and R. G. Hutchins, "Image-enhanced tracking," *IEEE Trans. Aerospace and Electronic Systems*, vol. AES-25, pp. 701–709, Sept. 1989.

[8] L. T. Bruton and Y. Zhang, "Applications of lossless MD structures for the filtering of digital image sequence," *Proc. IEEE ISCAS*, pp. 128–131, Jun. 1991.

[9] A. Fettweis, "Wave digital filters: theory and practice," *Proc. IEEE*, vol. 74, pp. 270–327, Feb. 1986.

[10] Y. Zhang and L. T. Bruton, "Differentiator-Type Three-Dimensional Recursive Ladder Filters Having Frequency Planar or Frequency Beam Shaped Passbands," *IEEE Trans. Circ. and Syst. for Video Technol.*, vol. ICSVT-2, pp. 297–305, Sept. 1992.

[11] A. Kummert, "Synthesis of 3D lossless first-order one ports with lumped elements," *IEEE Trans. Circuits Syst.*, vol. CAS-36, pp. 1445–1449, Nov. 1989.
[12] A. Kummert, "On the synthesis of multidimensional reactance multiports," *IEEE Trans. Circuits Syst.*, vol. CAS-38, pp. 637–642, Jun. 1991.
[13] J. K. Pitas and A. N. Venetsanopoulos, "The use of symmetries in the design of multidimensional digital filters," *IEEE Trans. Circuits Syst.*, vol. CAS-33, pp. 863–873, Sept. 1986.
[14] V. Rajaravivarma, P. K. Rajan and H. C. Reddy, "Planar symmetries in 3-D filter responses and their application in 3-D filter design," *IEEE Trans. Circuits Syst.*, vol. CAS-39, pp. 356–368, Jun. 1992.
[15] P. Agathoklis and L. T. Bruton, "Practical-BIBO stability of n-dimensional discrete systems," *Proc. Inst. Elec. Eng.*, vol. 130, pt. G, no. 6, pp. 236–242, Dec. 1983.
[16] T. J. Fowlow and L. T. Bruton, "Attenuation characteristics of three dimensional planar-resonant recursive digital filters," *IEEE Trans. Circuits Syst.*, vol. CAS-35, pp. 595–599, May 1988.
[17] F. F. Kuo, "Network Analysis and Synthesis," John Wiley & Sons, Inc., 1972.
[18] V. Oppenheim and R. W. Schafer, "Digital Signal Processing," pp. 137–148, Prentice-Hall, Inc., New Jersey, 1975.
[19] S. Chakrabarti and S. K. Mitra, "Design of two-dimensional digital filters via spectral transformations," *Proc. IEEE*, vol. 65, pp. 905–914, Jun. 1977.

Yuejin Zhang has received a B.Sc. degree in Control Engineering from Northeast University, China, in 1982, an M.Sc. degree in Optical Instrument Engineering from Zhejiang University, China, in 1984, an M.Sc. degree and a Ph.D. degree in Electrical and Computer Engineering from The University of Calgary, Canada, in 1991 and 1993, respectively.

Currently, he is with MacDonald, Dettwiler and Associates Ltd. in British Columbia, Canada. His research interests include signal processing, image sequence processing, real-time systems and circuits.

Leonard T. Bruton (M'71–SM'80–F'81) is a Professor of Electrical and Computer Engineering at The University of Calgary, Calgary, Alberta, Canada.

His research interests are in the areas of analog and digital signal processing. He is particularly interested in the design and implementation of microelectronic digital filters and the applications of multidimensional circuit and systems theory to digital image processing.